# Artificial Intelligence in Predicting Ocular Hypertension After Descemet Membrane Endothelial Keratoplasty

Min Seok Kim,[1] Heesuk Kim,[2] Hyung Keun Lee,[2] Chan Yun Kim,[2] and Wungrak Choi[2]

[1]Yonsei University College of Medicine, Seoul, Republic of Korea
[2]Institute of Vision Research, Department of Ophthalmology, Yonsei University College of Medicine, Seoul, Korea

Correspondence: Wungrak Choi, Institute of Vision Research, Department of Ophthalmology, Yonsei University College of Medicine, Gangnam Severance Hospital, 211 Eonju-ro, Gangnam-gu, Seoul 06273, Korea; wungrakchoi@yuhs.ac, wungrakchoi@hanmail.net.

**Received:** September 1, 2024
**Accepted:** December 30, 2024
**Published:** January 27, 2025

Citation: Kim MS, Kim H, Lee HK, Kim CY, Choi W. Artificial intelligence in predicting ocular hypertension after descemet membrane endothelial keratoplasty. *Invest Ophthalmol Vis Sci.* 2025;66(1):61. https://doi.org/10.1167/iovs.66.1.61

**Purpose.** Descemet membrane endothelial keratoplasty (DMEK) has emerged as a novel approach in corneal transplantation over the past two decades. This study aims to identify predisposing risk factors for post-DMEK ocular hypertension (OHT) and develop a preoperative predictive model for post-DMEK OHT.

**Methods.** Patients who underwent DMEK at Gangnam Severance Hospital between 2017 and 2024 were included in the study. Four machine learning models—XGBoost, random forest, CatBoost, and logistic regression—were trained to assess feature importance and develop a predictive classifier. An ensemble of these four models was used as the final predictive model. The ensemble model identified clinically significant patients for prediction or exclusion.

**Results.** A total of 106 eyes from patients who underwent DMEK were analyzed, with 31 eyes (29.2%) experiencing post-DMEK OHT. The final ensemble model achieved clinically significant classification for 61 eyes (57.5%) in the total patient population. Significant risk factors identified in all four models included angle recess area (ARA), best-corrected visual acuity, donor graft size, angle-to-angle distance, crystalline lens rise, and central corneal thickness. The average accuracy, precision, recall, area under the receiver operating characteristic curve, and area under the precision-recall curve values of the ensemble model obtained by a 5-fold cross-validation were 80.2%, 60.0%, 59.7%, 82.3%, and 68.0%, respectively.

**Conclusions.** This study identified significant risk factors for post-DMEK OHT and highlighted the importance of ocular topographic measures in risk assessment. The development of a final machine learning model to differentiate between clinically predictable patient groups demonstrates the clinical utility of the proposed model for predicting post-DMEK OHT.

Keywords: descemet membrane endothelial keratoplasty, ocular hypertension, glaucoma, optical coherence tomography, machine learning

Corneal transplantation is one of the most frequently performed transplantations worldwide, and its prevalence continues to rise.[1] Conventionally, penetrating keratoplasty (PKP) has been the singular transplantation option for severe corneal disorders. However, in the past two decades, posterior lamellar keratoplasty, exemplified by procedures such as Descemet membrane endothelial keratoplasty (DMEK) or Descemet stripping automated endothelial keratoplasty, has emerged as a viable alternative to PKP for treating corneal endothelial disorders due to its lower complication rates.[2,3]

Glaucoma, along with graft rejection, constitutes a critical complication after corneal transplantation, as a common cause for graft failure and the leading cause of vision loss after keratoplasty.[1,4] Although the management of graft rejection dramatically advanced with the introduction of posterior lamellar keratoplasty techniques, many limitations still exist in the prediction and risk management of post-keratoplasty glaucoma.[5] Post-penetrating keratoplasty glaucoma is recognized as the most common cause of post-keratoplasty glaucoma, and several studies have scrutinized its associated risk factors.[6–8] In contrast, research on post-DMEK glaucoma remains relatively sparse despite its significance as a serious complication after DMEK.[9–11] Moreover, existing studies often focus on postoperative factors in assessing the risk of post-penetrating keratoplasty glaucoma, thereby hindering the development of preoperative prediction models for post-keratoplasty glaucoma.[7]

Machine learning (ML) presents a promising approach for addressing multivariate challenges across various fields. The applicability of ML models to glaucoma prediction has also been widely studied, given the complexity of the potential associated risk factors.[12,13] Although deep-learning-powered artificial intelligence (AI) has shown impressive performance, traditional ML models remain extensively studied for clinical predictions, primarily because of their more interpretable model structures.[14]

The risk factors previously considered important for post-keratoplasty glaucoma include certain categorical conditions such as history of glaucoma, graft failure, aphakic lens status,

or history of vitrectomy.[4,15] Meanwhile, biometric features specific to each eye were overlooked despite their diagnostic significance in glaucoma.[16,17]

This study aimed to elucidate the predisposing risk factors for post-DMEK ocular hypertension (OHT) and propose a preoperative predictive model incorporating anterior segment ocular topographic measurements obtained through anterior segment optical coherence tomography (AS-OCT). We evaluated the significance of each risk factor in post-DMEK OHT using various ML models for classification and survival analysis. Based on these models, we constructed a final preoperative ensemble model for predicting post-DMEK OHT and verified its performance and potential significance for clinical use.

## Methods

### Study Design

This retrospective institutional analytical study adhered to the principles outlined in the Declaration of Helsinki and was approved by the Institutional Review Board of Severance Hospital, Yonsei University College of Medicine (Approval number: 3-2024-0058). This study was granted a waiver of informed consent.

We reviewed 124 eyes of 119 patients who underwent DMEK at Gangnam Severance Hospital between December 2017 and January 2024. Eyes with a minimum follow-up period of one month were included, whereas those undergoing PKP as a reoperation were excluded.

### Data Collection

Comprehensive medical records were assessed, including demographics, medical and surgical histories, lens status, indication for DMEK, preoperative best-corrected visual acuity (BCVA), history of glaucoma, donor graft size, number of re-bubbling and reoperation procedures, and intraocular pressure (IOP) (Fig. 1a). All features were measured preoperatively, with IOP continuously monitored post-DMEK during the follow-up.

AS-OCT (CASIA; Tomey, Nagoya, Japan) was performed on all eyes to obtain biometric measurements, including central corneal thickness (CCT), crystalline lens rise (CLR), angle-to-angle (ATA) distance, anterior chamber

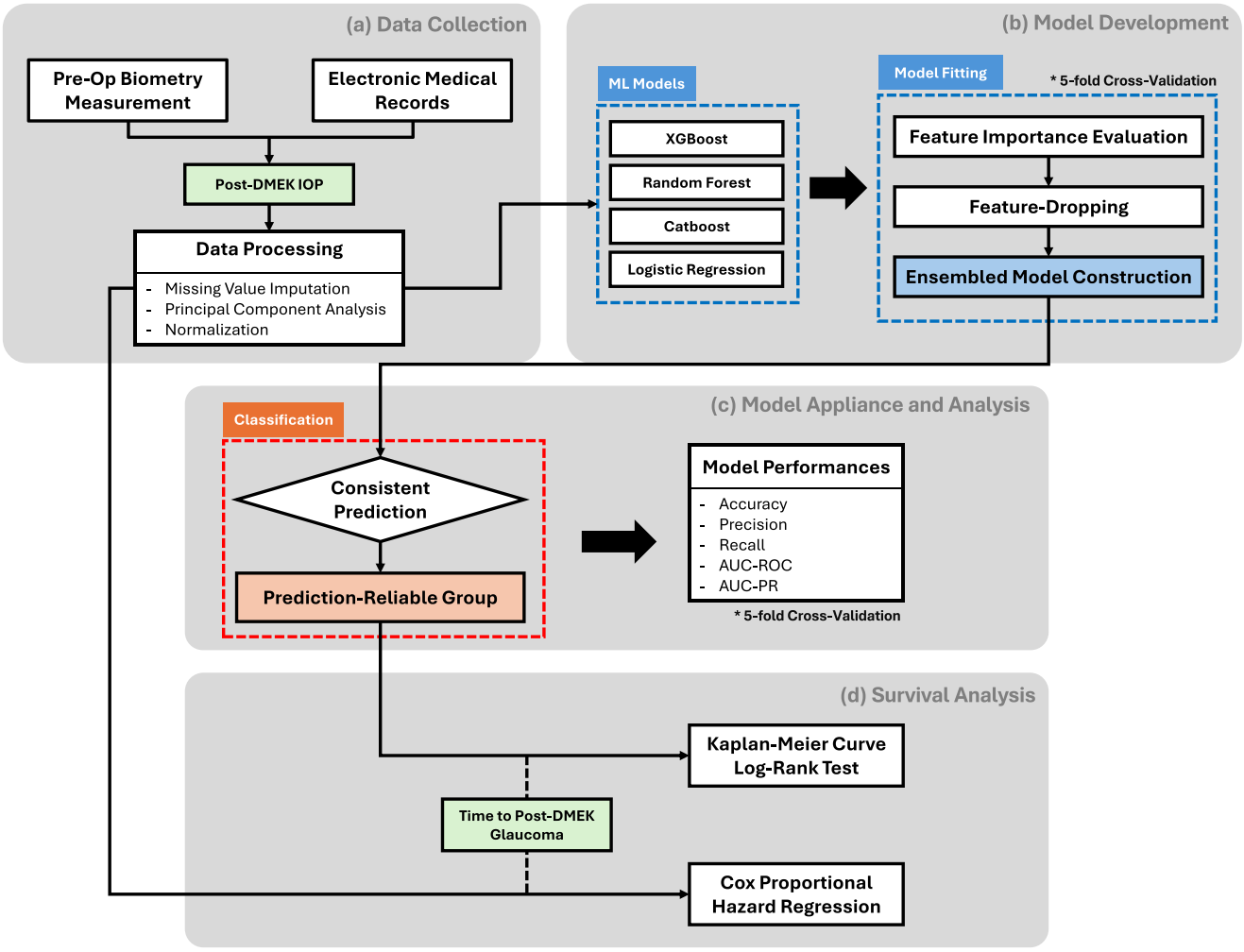


**Figure 1.** Workflow diagram of the study. **(a)** Data collection and processing of preoperative biometric measurements, preoperative electronic medical records, and pre- and post-DMEK intraocular pressure. **(b)** Development of an ensemble predictive model with four selected machine-learning models. **(c)** Application of the final model and estimation of the model performance. **(d)** Survival analysis of the cohort with Kaplan–Meier curve, log-rank test, and Cox proportional hazard regression. AUC-PR, area under the precision-recall curve; op, operation.

Investigative Ophthalmology & Visual Science

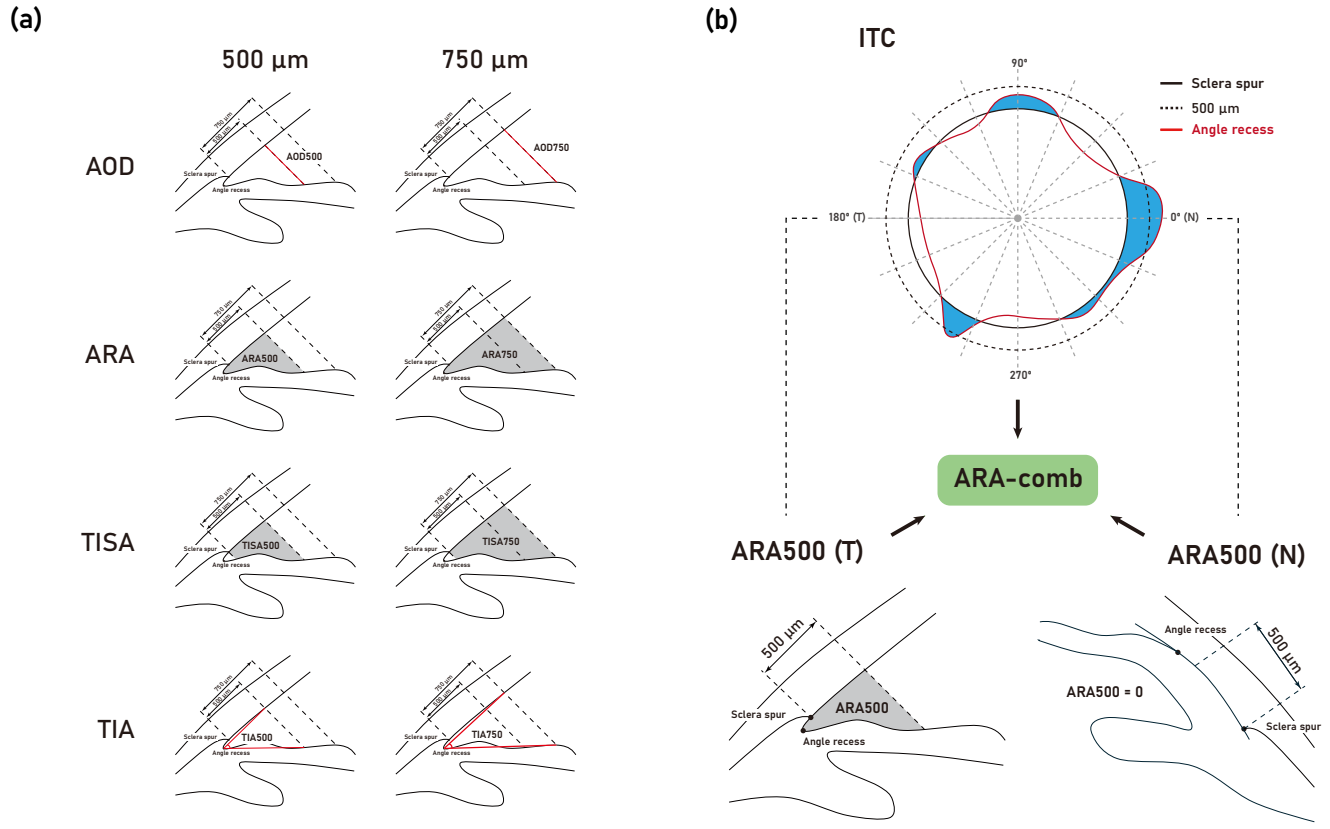


**Figure 2.** Estimation of AS-OCT-obtained topographic variables. **(a)** Schematic demonstration of AOD, ARA, TISA, and TIA measured at 500 µm and 750 µm from the sclera spur. **(b)** Visual explanation of measuring ITC and ARA500. ARA500 was measured in the nasal and temporal parts of each eye. The coronal plane of the right eye is selected to explain the ITC index. As a representative measure of the anterior chamber angle, ITC, nasal ARA500, and temporal ARA500 were integrated with the principal component analysis method to form a novel variable, ARA-comb.

depth (ACD), anterior chamber width (ACW), axial length, angle recess area (ARA), angle opening distance (AOD), trabecular-iris space area (TISA), and trabecular-iris angle (TIA) (Fig. 1a). ARA, AOD, TISA, and TIA were measured at 500 µm and 750 µm from the scleral spur (Fig. 2a).

OHT after DMEK was defined by an IOP $\geq$ 22 mm Hg or an increase in IOP of over 10 mm Hg from preoperative values. To rule out IOP elevation caused by undetached grafts, postoperative IOP elevations occurring at least 30 days after the last surgery or re-bubbling were considered.

Among ARA, AOD, TISA, and TIA, only ARA500 was selected for analysis because they showed high correlations with each other. ARA combined with iridotrabecular contact (ARA-comb), an integrated variable of ARA500 and iridotrabecular contact (ITC) with principal component analysis, was subsequently derived as a representative measure of the anterior chamber angle (Fig. 2b).

## Surgical Technique

The donor cornea was cut from the endothelial side with trephine. Standard preoperative preparation was performed after topical anesthesia. All the procedures were conducted by a single, experienced surgeon. After widening the eyelid fissure with a speculum, a peripheral iridectomy was performed inferotemporally. Centering was achieved with calipers. Eight radial markings were drawn using radial keratotomy. The Descemet membrane was scored peripherally using a reverse Terry-Sinskey hook and then peeled from the overlying stroma. An incision was made using a keratome at the 12 o'clock position, and the membrane was removed using forceps. A preloaded Descemet membrane was prepared from the donor cornea and applied to the recipient bed with a DORC tube. The tube tip was inserted into the corneal incision, and the donor tissue was injected into the anterior chamber. The anterior surface of the cornea was gently tapped and swiped until the graft was precisely positioned and unscrolled. SF6 gas was injected into the anterior chamber for 30 minutes to induce adhesion. At the end of the procedure, ointments were applied, and the eyes were firmly patched.

## Statistical Analysis

Data were analyzed using SPSS Statistics version 26 (IBM, Armonk, NY, USA). Baseline characteristics were compared between healthy individuals and patients with OHT. Student's *t*-test was used for continuous variables, and the $\chi^2$ test or Fisher's exact test was used for categorical variables, whenever appropriate.

## Model Development

The collected data were subsequently reformatted into a set of predictors consisting of medical records and biomet-

Investigative Ophthalmology & Visual Science

ric measures. Incidence and time to occurrence of post-DMEK OHT were recorded as target values. Missing values were imputed with the mean of each variable. Missing values for each parameter did not exceed 10% of the total dataset. To elucidate significant risk factors, ML models were trained and underwent feature importance evaluation. The entire dataset with data imbalance addressed using the synthetic minority oversampling technique was used. Four top-performing ML models—XGBoost, random forest, CatBoost, and logistic regression— were selected for training. In logistic regression model, estimated *P* values were used for feature importance assessment. Based on the evaluated feature importance, each model was subjected to feature dropping to determine the optimal combination of predictors that demonstrated the best model performance. Model performance was evaluated by stratified 5-fold cross-validation (Fig. 1b). Each patient was included in the test set for one fold and in the training set for the remaining four folds, maintaining an 80%/20% train-test split across folds. To the training set of each fold, synthetic minority oversampling technique was applied to handle imbalanced datasets.

### Model Application and Analysis

All eyes in the cohort were predicted using the four trained ML models. Based on this prediction, an ensemble of the XGBoost, random forest, CatBoost, and logistic regression models was used to select a reliable group with significant predictability for post-DMEK OHT incidence, where glaucoma predictions were consistently positive or negative across the four models (Fig. 1c). To prevent overfitting, each dataset was predicted using ML models trained on datasets that did not include themselves through stratified 5-fold cross-validation. The performance of the ensemble model was estimated for the selected prediction-reliable group using the average of the results throughout the five folds. Probability of the logistic regression model, which had the highest area under the receiver operating characteristic curve (AUC-ROC) as a single model, was used to calculate the AUC-ROC and the area under the precision-recall curve (AUC-PR) of the model for the selected group.

### Survival Analysis

Time-wise incidence of post-DMEK OHT was obtained for survival analysis. Postoperative days of post-DMEK OHT after primary DMEK were measured, and censoring occurred at the last visit. For a time-wise investigation of feature importance, a multivariate Cox proportional hazards regression model was conducted to estimate variables significantly associated with post-DMEK OHT in terms of survival analysis.

For the ML-obtained significantly predictable group, Kaplan–Meier curves and log-rank test were performed to analyze the differences in survival rates between the positive and negative prediction groups (Fig. 1d). Because the longest failure time was 778 days, all data were collectively censored on day 800 for better visualization.

## Results

### Dataset Characteristics

A total of 106 eyes of 101 patients were included in this study, with 31 eyes (29.2%) showing elevated IOP after DMEK. All eyes had a minimum follow-up of 1 month, with a mean follow-up period of 42.1 ± 17.8 months. The cohort had a mean age of 59.9 ± 14.1 years, with 52 eyes (49.1%) belonging to female patients. The primary etiologies for DMEK included Fuchs' endothelial corneal dystrophy (FECD) in 16 eyes (15.1%), pseudophakic bullous dystrophy in 74 eyes (69.8 %), and other indications in 16 eyes (15.1 %). Table 1 summarizes the demographic characteristics.

Among the predictors, BCVA, etiology, CCT, ARA-comb, and ACW exhibited the highest correlation with post-DMEK OHT incidence (Fig. 3a). The correlation matrix of the biometric measures revealed no significant collinearity among variables, with the highest correlation coefficient of 0.53 observed between ARA-comb and ACD (Fig. 3b).

### Feature Importance Evaluation

The feature importance of XGBoost, random forest, CatBoost, and logistic regression model was evaluated (Fig. 4). ATA, ARA-comb, CCT, and BCVA were highly ranked across XGBoost, random forest, and CatBoost, whereas donor graft size and ARA-comb were the most significant variables in logistic regression model (Table 2).

### Model Construction and Prediction-Reliable Group Selection

Table 3 presents the final selected features for each model. ARA-comb and BCVA remained in all four models after feature-dropping, while donor graft size, ATA, CLR, and CCT were included in three of the final modified models. Using

**Table 1.** Baseline Characteristics of the Dataset

| | Normal Group | Postoperative OHT Group | Total | *P* Value |
|---|---|---|---|---|
| Number of cases | 75 (70.8%) | 31 (29.2%) | 106 (100%) | — |
| Follow-up time, month (SD) | 18.9 (15.2) | 27.1 (19.6) | 21.2 (17.0) | 0.043* |
| Patient age, year (SD) | 61.0 (13.5) | 57.3 (15.4) | 59.8 (14.1) | 0.214 |
| Female sex | 39 (52%) | 13 (41.9%) | 52 (49.1%) | 0.346 |
| Right eye | 26 (34.7%) | 19 (61.3%) | 45 (42.5%) | 0.012* |
| Etiology | | | | |
| FECD | 12 (16%) | 4 (12.9%) | 16 (15.1%) | 0.230 |
| PBK | 49 (65.3%) | 25 (80.6%) | 74 (69.8%) | |
| Other | 14 (18.7%) | 2 (6.5%) | 16 (15.1%) | |
| Phakic eyes | 31 (41.3%) | 11 (35.5%) | 42 (39.6%) | 0.663 |

FECD, Fuchs' endothelial corneal dystrophy; PBK, pseudophakic bullous keratopathy; SD, standard deviation.

Overall, 31 (29.2%) of 106 eyes experienced intraocular pressure elevation after DMEK. The *P* value of each feature between the normal and IOP-elevated groups are shown in the table.

* Statistical significance.

Investigative Ophthalmology & Visual Science

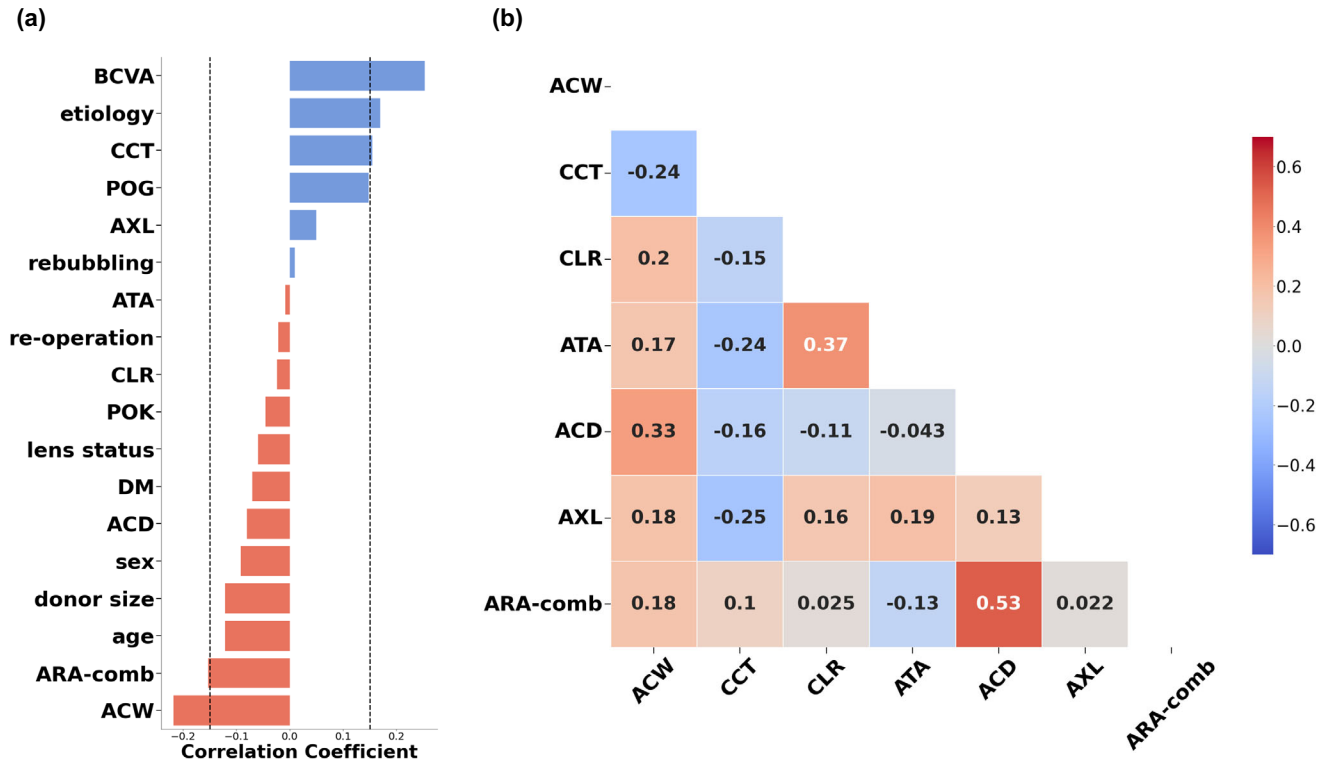


**Figure 3.** Correlations among the variables of the dataset. **(a)** The correlation coefficient between predictors and postoperative OHT incidence. The variables were aligned in a descending manner. The correlation coefficient of ± 0.15 was marked with a dashed line. BCVA, etiology, CCT, ARA-comb, and ACW showed the highest correlation with postoperative OHT. **(b)** Correlation matrix between topographic variables. No notable collinearity was observed between the variables. AXL, axial length; DM, diabetes mellitus history; POG, preoperative glaucoma incidence; POK, preoperative keratoplasty history.

these selected features for training, the AUC-ROC values of the ML models, XGBoost, random forest, CatBoost, and logistic regression, were 64.9%, 65.4%, 67.7%, and 73.5%, respectively.

According to predictions by the ensemble model of the four ML models, 61 eyes (57.5%) of the 106 eyes were identified as reliable. Among these, 11 eyes (18.0%) were predicted positive for post-DMEK OHT across all models, whereas 50 eyes (82.0%) were predicted negative. The average accuracy, precision, recall, AUC-ROC, and AUC-PR values of the ensemble model obtained by a 5-fold cross-validation were 80.2%, 60.0%, 59.7%, 82.3%, and 68.0%, respectively, representing a significant enhancement in performance compared to the individual ML models (Supplementary Fig. S1). Among the four ML models, no single model caused a notable performance change compared to the other ML models when excluded from the ensemble, indicating that each model contributed evenly to the ensemble model (Supplementary Table S1).

### Survival Analysis

*P* values of each feature in the ensemble model were estimated with the Cox proportional hazards model. Only ACW exhibited a significant association ($P < 0.05$) (Table 4). The Kaplan–Meier curve of the ensemble model is shown in Figure 5. The estimated *P* value obtained using the log-rank test demonstrated a significant difference between the two groups ($P = 0.0089$).

## Discussion

Glaucoma is associated with multiple risk factors, highlighting the necessity of an ML-based approach for glaucoma prediction, as suggested in several studies.[12,18,19] However, to the best of our knowledge, no previous study has introduced ML models specifically to predict post-keratoplasty glaucoma. Previous investigations assessing the risk factors for post-keratoplasty glaucoma primarily relied on retrospective statistical analyses, often incorporating postoperative values. Although valuable for understanding the roles of individual factors in glaucoma pathogenesis, these studies may not be suitable for preoperative glaucoma prediction.

In this study, the significance of each risk factor in predicting post-DMEK OHT was evaluated using four selected ML models. Each model underwent feature selection and was combined to develop the final prediction model. Among the 106 eyes, consistent predictions were obtained from all four ML models within the final ensemble model for 61 eyes. The ensemble model demonstrated reliable performance, achieving an average accuracy of 80.2% and an AUC-ROC of 82.3% in the selected prediction-reliable group. Furthermore, the survival analysis of this group revealed significant differences in hazard ratios between each predicted group. These findings underscore the reliability of our ML models for predicting post-DMEK OHT based on a retrospectively collected dataset.

In the pathophysiology of glaucoma, disrupted drainage of the aqueous humor, especially in the trabecular mesh-

Investigative Ophthalmology & Visual Science

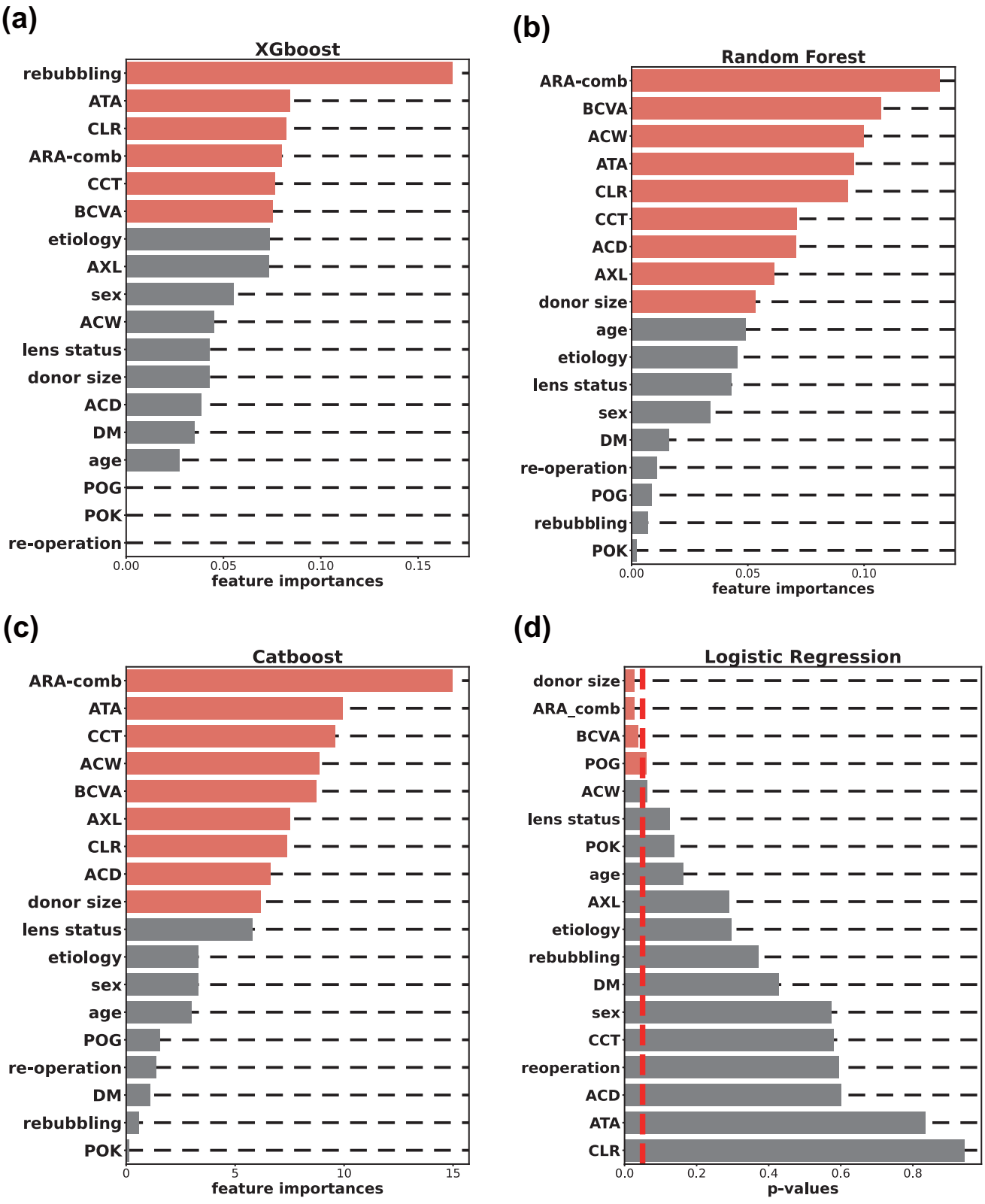


**Figure 4.** Feature importance of the (**a**) XGBoost, (**b**) random forest, (**c**) CatBoost, and (**d**) logistic regression models. Information gain and GINI importance were used for feature importance assessment in XGBoost and random forest respectively. For CatBoost, feature importance was automatically estimated using catboost python package based on prediction value change and loss function change. The feature significance in the logistic regression model is estimated with the *P* value of each variable, with $P = 0.05$ marked in *red*. The ML models were subjected with feature dropping for better model performances, and the final selected features in each model are colored *orange*. AXL, axial length; DM, diabetes mellitus history; POG, preoperative glaucoma incidence; POK, preoperative keratoplasty history.

Investigative Ophthalmology & Visual Science

**Table 2.** Feature Evaluation Using the Multiple Logistic Regression Model

| | Coefficient | SE | *P* Value |
|---|---|---|---|
| Donor size | −0.5328 | 0.242 | 0.027* |
| ARA-comb | −0.6443 | 0.293 | 0.028* |
| BCVA | 0.5548 | 0.269 | 0.039* |
| Preoperative glaucoma | 0.4554 | 0.244 | 0.062 |
| ACW | −0.536 | 0.287 | 0.062 |
| Lens status | −0.4816 | 0.314 | 0.125 |
| Preoperative keratopathy | −0.3924 | 0.264 | 0.137 |
| Age | −0.3752 | 0.27 | 0.164 |
| AXL | 0.2825 | 0.268 | 0.291 |
| Etiology | 0.2511 | 0.241 | 0.297 |
| Re-bubbling | 0.2042 | 0.229 | 0.372 |
| DM | −0.2115 | 0.267 | 0.428 |
| Sex | −0.143 | 0.254 | 0.574 |
| CCT | −0.1664 | 0.301 | 0.58 |
| Reoperation | −0.1372 | 0.258 | 0.595 |
| ACD | 0.1779 | 0.341 | 0.602 |
| ATA | 0.0574 | 0.275 | 0.835 |
| CLR | 0.019 | 0.266 | 0.943 |

AXL, axial length; DM, diabetes mellitus history; SE, standard error.
* Statistical significance.

**Table 3.** Final Selected Variables for the XGBoost, Random Forest, CatBoost, and Logistic Regression Models

| ML Models | Selected Variables |
|---|---|
| XGBoost | Re-bubbling, ATA, CLR, ARA-comb, CCT, BCVA |
| Random Forest | ARA-comb, BCVA, ACW, ATA, CLR, CCT, ACD, AXL, donor size |
| CatBoost | ARA-comb, ATA, BCVA, CCT, ACW, AXL, CLR, ACD, donor size |
| Logistic regression | Donor size, BCVA, ARA-comb, preoperative glaucoma |

AXL, axial length.
All models included ARA-comb and BCVA as significant predictors. Donor graft size, ATA, CLR, and CCT were selected in three of the models.

**Table 4.** The *P* Value of Each Covariate Obtained From the Multivariate Cox Proportional Hazards Regression Model

| Features | *P*-Value |
|---|---|
| ACW | 0.016* |
| BCVA | 0.086 |
| AXL | 0.142 |
| Pre-op keratopathy | 0.196 |
| Pre-op glaucoma | 0.210 |
| Re-operation | 0.215 |
| ARA-comb | 0.254 |
| Lens status | 0.256 |
| DM | 0.507 |
| ATA | 0.547 |
| Sex | 0.661 |
| Etiology | 0.714 |
| ACD | 0.728 |
| CLR | 0.787 |
| CCT | 0.813 |
| Age | 0.893 |
| Donor size | 0.928 |
| Re-bubbling | 0.948 |

AXL, axial length; DM, diabetes mellitus history; op, operation.
* Statistical significance.

work, is a leading cause of the condition's progression.[20] The drainage pathway relies heavily on the anatomical structure of the anterior segment, and several studies have analyzed AS-OCT-obtained topographic measurements of the anterior segment as crucial predictors of glaucoma.[21,22] However, these biometric variables are often neglected in the retrospective analyses of patients with glaucoma after corneal transplantation.

The variables for the prediction in our study consisted of two groups; demographic information and topographic biometric measurements obtained retrospectively from electronic medical records and AS-OCT. Based on the evaluated feature importance, ARA-comb, BCVA, donor graft size, ATA, CLR, and CCT were significantly selected in more than three of the four trained ML models, including risk factors derived from both medical records and biometric measurements. Among the biometric measurements, ARA-comb, an integrated variable of ARA and ITC, was selected as the most influential predictor among all four models.

Reduction in the anterior chamber angle directly contributes to glaucoma pathogenesis as it induces obstruction of the drainage pathway of the aqueous humor, leading to angle-closure glaucoma.[23] Assessment of this angle obstruction requires a multidimensional approach, since both the extent of the obstructed area and the severity of constriction at each location contribute to the reduced outflow of the aqueous humor. In the present study, we introduced two different variables, ARA and ITC, which are topographic variables obtained with AS-OCT, for a comprehensive assessment of obstruction. AOD, ARA, TISA, and TIA, the biometric variables obtained with AS-OCT, can indicate the severity of obstruction in different sections, as their values diminish proportionally with the narrowing of the angle. Specifically, ARA measures the triangular area from the angle recess to the AOD and thus comprehends the topographic characteristics near the trabecular meshwork. Conversely, the ITC index, which is the coronally measured proportion of the area with iridotrabecular contact, offers a comprehensive measure of angle closure across the entire eye. Taken together, the substantial significance of ARA-comb suggests that integrating ARA and ITC provides a comprehensive understanding of the extent of angle closure.

In PKP, transplant size and suturing techniques are closely associated with postoperative IOP elevation. Zimmerman et al.[24] identified that a donor graft with a 0.5-mm larger button than the recipient bed significantly lowered IOP levels after PKP, as shorter donor grafts induce compression that leads to the collapse of iridocorneal angles. The graft compression is associated with the relative length between the donor graft and recipient bed. Among the topographic variables, ATA, which quantifies the distance between the iridocorneal angles, directly reflects the size of the host corneal bed. Therefore, the notable significance of donor graft size and ATA in the ML models suggests that a relatively small donor graft to the recipient cornea may provoke ocular compression, not only in PKP but also in DMEK.

In addition to these conventional risk factors, potential prognostic biomarkers such as CCT or BCVA also showed significance in our ensemble model. The prognostic significance of CCT in OHT and glaucoma progress has been well established.[25,26] Belovay and Goldberg[26] found that a thinner CCT was associated with the progression of primary open-angle glaucoma in patients with OHT. However, considering that variables indicative of angle closure as a primary cause

Investigative Ophthalmology & Visual Science

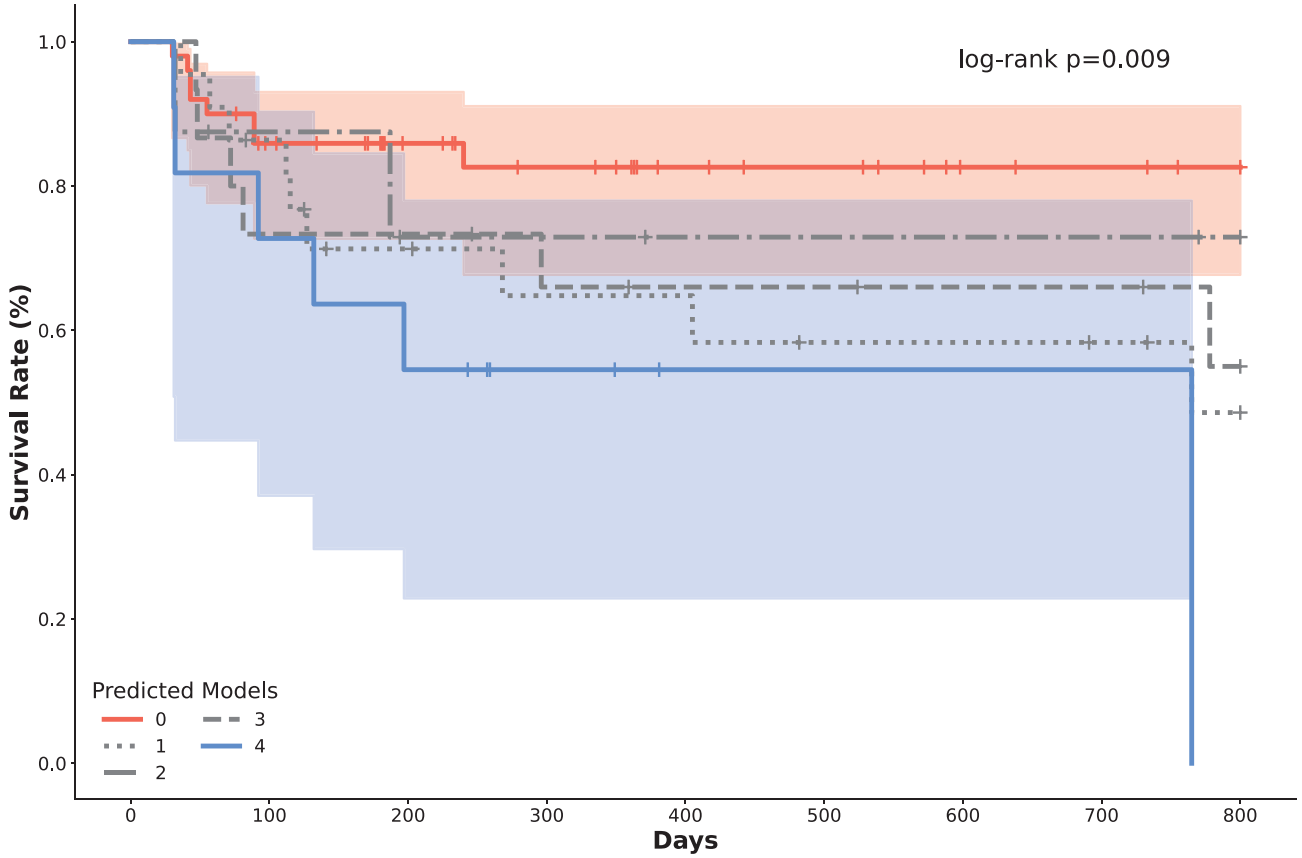


**Figure 5.** Kaplan–Meier curve of the cohort. Each eye was predicted using the XGBoost, random forest, CatBoost, and logistic regression models and classified based on the number of positively predicted models among the four models. Groups with consistent predictions, with no positively predicted models or with four positively predicted models, are indicated in *orange* and *blue*, respectively. The log-rank test between two groups that were predicted positive and negative unanimously in the four models resulted in a $P$ value = 0.0089.

for post-DMEK OHT, such as ARA-comb and graft donor size, were significant in our ensemble model, the implications of CCT should be interpreted attentively. Moreover, our dataset included eyes with abnormally elevated preoperative CCT, likely due to corneal edema from endothelial disorders, further complicating the connection between CCT and post-DMEK OHT. Meanwhile, the correlation between visual acuity and OHT is also uncertain. Although visual acuity is a critical prognostic parameter affected by glaucoma, research on its application in predicting glaucoma or OHT is limited. Thus the precise role of CCT and BCVA in predicting post-DMEK OHT remains unresolved in this study and requires further investigation.

Post-keratoplasty OHT is a primary cause of graft failure and vision loss; therefore various studies have emphasized the importance of pre and postoperative monitoring of IOP levels for early detection of the condition.[27,28] However, early postoperative IOP monitoring is often hindered by factors such as corneal thickening, irregular surfaces, and scarring.[28] Consequently, methods for assessing the risk of glaucoma preoperatively are urgently needed. Moreover, preoperative awareness of the risk of glaucoma can greatly support treatment planning after transplantation. For instance, corticosteroids are commonly administered post-keratoplasty despite their potential to elevate IOP.[27,29] Classifying patients based on preoperative risk estimates can facilitate personalized postoperative treatments, including intensified IOP monitoring and targeted medication, such as prostaglandin eye drops. Therefore our ensemble model, which provides preoperative prediction and patient classification, offers substantial clinical advantages for enhancing postoperative treatment planning.

When selecting the ML models for analysis, we considered models capable of feature importance analysis and suitable for supervised learning. Alongside the four ML models analyzed in our study, a support vector machine with a linear kernel and a decision tree model were also trained for prediction. However, these models were excluded because of their poor performance.

A limitation of our study is its retrospective and single-institution dataset, with some prognostic markers of keratoplasty, such as endothelial cell density, unavailable for analysis due to incomplete recordings.[30] Further prospective studies are required to assess the risks associated with these features. Additionally, the cohort size was constrained by data collection from a single institution. AI models based on deep learning have outperformed traditional ML models in terms of predictive accuracy. In particular, explainable AI models provide feature importance evaluation and have been employed in predicting various conditions, including acute appendicitis, non-alcoholic fatty liver disease, hepatitis, and stroke.[31–34] Despite these advantages, deep learning models could not be used in this study since training deep learning-based AI models requires larger datasets to mitigate

overfitting. Therefore further studies with larger datasets, such as those with extended follow-up or multi-institutional data, should be conducted to explore explainable AI models for more precise risk factor analysis and prediction. Furthermore, our study primarily targeted to develop a preoperative screening model, which may contribute to a higher false-positive rate, particularly considering the use of mean imputation for handling missing data. This limitation also underscores the importance of further validation using larger datasets to refine predictive accuracy and ensure the robustness of the model.

In summary, we developed an ensemble ML model for predicting post-DMEK OHT. The topographic variables obtained with AS-OCT were identified as significant predisposing risk factors. The ensemble model effectively stratified patients into the high- and low-risk groups for postoperative OHT, and survival analysis demonstrated significant differences between these groups. Although the specific roles of several risk factors require further investigation, the preoperative risk assessment of post-DMEK OHT can guide tailored postoperative treatments and reduce complications.

## *Acknowledgments*

Supported by the Basic Science Research Program through the National Research Foundation of Korea (NRF-2022R1I1A1A01071919 & RS-2024-00405287) and a research grant from Gangnam Severance Hospital (D-2023-0012 & 3-2024-0002). The sponsor or funding organization had no role in the design or conduct of this research.

**Author Contributions:** M.S.K.: supervision, modeling, investigation, data analysis, and writing; H.K.: investigation, data analysis, and writing; H.K.L.: data analysis and validation; C.Y.K.: modeling, methodology, and investigation; W.C.: supervision, methodology, modeling, and validation. All authors jointly interpreted the findings and wrote, revised, and approved the final manuscript.

Disclosure: **M.S. Kim**, None; **H. Kim**, None; **H.K. Lee**, None; **C.Y. Kim**, None; **W. Choi**, None

## *References*

1. Anders LM, Gatzioufas Z, Grieshaber MC. Challenges in the complex management of post-keratoplasty glaucoma. *Ther Adv Ophthalmol*. 2021;13:25158414211031397.
2. Yeu E, Gomes JAP, Ayres BD, et al. Posterior lamellar keratoplasty: techniques, outcomes, and recent advances. *J Cataract Refract Surg*. 2021;47:1345–1359.
3. Kim M, Kim KH, Lee HK. Clinical outcomes of descemet membrane endothelial keratoplasty using a preloaded imported graft. *Korean J Ophthalmol*. 2023;37:373–379.
4. Ayyala RS. Penetrating keratoplasty and glaucoma. *Surv Ophthalmol*. 2000;45:91–105.
5. Yin J. Advances in corneal graft rejection. *Curr Opin Ophthalmol*. 2021;32:331–337.
6. Kirkness CM, Moshegov C. Post-keratoplasty glaucoma. *Eye*. 1988;2:S19–S26.
7. Shree N, Gandhi M, Dave A, Mathur U. Incidence and risk factors for post-penetrating keratoplasty glaucoma. *Indian J Ophthalmol*. 2022;70:1239–1245.
8. Wu S, Xu J. Incidence and risk factors for post-penetrating keratoplasty glaucoma: a systematic review and meta-analysis. *PLoS One*. 2017;12:e0176261.
9. Maier AB, Pilger D, Gundlach E, Winterhalter S, Torun N. Long-term results of intraocular pressure elevation and post-DMEK glaucoma after Descemet membrane endothelial keratoplasty. *Cornea*. 2021;40:26–32.
10. Maier AK, Wolf T, Gundlach E, et al. Intraocular pressure elevation and post-DMEK glaucoma following Descemet membrane endothelial keratoplasty. *Graefes Arch Clin Exp Ophthalmol*. 2014;252:1947–1954.
11. Ang M, Sng CCA. Descemet membrane endothelial keratoplasty and glaucoma. *Curr Opin Ophthalmol*. 2018;29:178–184.
12. Bowd C, Goldbaum MH. Machine learning classifiers in glaucoma. *Optom Vis Sci*. 2008;85:396–405.
13. Barros DMS, Moura JCC, Freire CR, Taleb AC, Valentim RAM, Morais PSG. Machine learning applied to retinal image processing for glaucoma detection: review and perspective. *Biomed Eng Online*. 2020;19:20.
14. Oh S, Park Y, Cho KJ, Kim SJ. Explainable machine learning model for glaucoma diagnosis and its interpretation. *Diagnostics (Basel)*. 2021;11:510.
15. Chanbour W, Ayoub MH, Towair E, et al. Incidence, risk factors and treatment outcomes of intraocular hypertension and/or glaucoma post-penetrating keratoplasty: a 5-year Lebanese retrospective descriptive study. *Clin Ophthalmol*. 2020;14:2497–2505.
16. Mohammadzadeh V, Cheng M, Zadeh SH, et al. Central macular topographic and volumetric measures: new biomarkers for detection of glaucoma. *Transl Vis Sci Technol*. 2022;11:25.
17. Choi W, Kim JD, Bae HW, Kim CY, Seong GJ, Kim M. Axial length as a risk factor for steroid-induced ocular hypertension. *Yonsei Med J*. 2022;63:850–855.
18. Fernandez Escamez CS, Martin Giral E, Perucho Martinez S, Toledano Fernandez N. High interpretable machine learning classifier for early glaucoma diagnosis. *Int J Ophthalmol*. 2021;14:393–398.
19. Wu JH, Nishida T, Weinreb RN, Lin JW. Performances of machine learning in detecting glaucoma using fundus and retinal optical coherence tomography images: a meta-analysis. *Am J Ophthalmol*. 2022;237:1–12.
20. Weinreb RN, Aung T, Medeiros FA. The pathophysiology and treatment of glaucoma: a review. *JAMA*. 2014;311:1901–1911.
21. Fu H, Xu Y, Lin S, et al. Segmentation and quantification for angle-closure glaucoma assessment in anterior segment OCT. *IEEE Trans Med Imaging*. 2017;36:1930–1938.
22. Kim KN, Lim HB, Lee JJ, Kim CS. Influence of biometric variables on refractive outcomes after cataract surgery in angle-closure glaucoma patients. *Korean J Ophthalmol*. 2016;30:280–288.
23. Sun X, Dai Y, Chen Y, et al. Primary angle closure glaucoma: what we know and what we don't know. *Prog Retin Eye Res*. 2017;57:26–45.
24. Zimmerman T, Olson R, Waltman S, Kaufman H. Transplant size and elevated intraocular pressure. Postkeratoplasty. *Arch Ophthalmol*. 1978;96:2231–2233.
25. Sng CC, Ang M, Barton K. Central corneal thickness in glaucoma. *Curr Opin Ophthalmol*. 2017;28:120–126.
26. Belovay GW, Goldberg I. The thick and thin of the central corneal thickness in glaucoma. *Eye (Lond)*. 2018;32:915–923.
27. Kornmann HL, Gedde SJ. Glaucoma management after corneal transplantation surgeries. *Curr Opin Ophthalmol*. 2016;27:132–139.
28. Reinhard T, Kallmann C, Cepin A, Godehardt E, Sundmacher R. The influence of glaucoma history on graft survival after penetrating keratoplasty. *Graefes Arch Clin Exp Ophthalmol*. 1997;235:553–557.
29. Goldberg DB, Schanzlin DJ, Brown SI. Incidence of increased intraocular pressure after keratoplasty. *Am J Ophthalmol*. 1981;92:372–377.

30. Ku BI, Hsieh YT, Hu FR, Wan IJ, Chen WL, Hou YC. Endothelial cell loss in penetrating keratoplasty, endothelial keratoplasty, and deep anterior lamellar keratoplasty. *Taiwan J Ophthalmol*. 2017;7:199–204.
31. Akbulut S, Yagin FH, Cicek IB, Koc C, Colak C, Yilmaz S. Prediction of perforated and nonperforated acute appendicitis using machine learning-based explainable artificial intelligence. *Diagnostics*. 2023;13:1173.
32. Sorino P, Campanella A, Bonfiglio C, et al. Development and validation of a neural network for NAFLD diagnosis. *Sci Rep*. 2021;11:20240.
33. Peng J, Zou K, Zhou M, et al. An Explainable Artificial Intelligence Framework for the Deterioration Risk Prediction of Hepatitis Patients. *J Med Syst*. 2021;45:61.
34. Islam MS, Hussain I, Rahman MM, Park SJ, Hossain MA. Explainable artificial intelligence model for stroke prediction using EEG signal. *Sensors*. 2022;22:9859.